EFFECT OF THE TiO_2 PRECURSOR PHASE ON THE SYNTHESIS OF TiO_2-BLACK-IMPREGNATED ELECTRODES IN THE DEGRADATION OF ACETAMINOPHEN SOLUTIONS

DANIEL SOLARTE FERRO

UNIVERSITY OF VALLE
FACULTY OF ENGINEERING
SCHOOL OF CHEMICAL ENGINEERING
SANTIAGO DE CALI
2025

EFFECT OF THE TiO_2 PRECURSOR PHASE ON THE SYNTHESIS OF TiO_2-BLACK-IMPREGNATED ELECTRODES IN THE DEGRADATION OF ACETAMINOPHEN SOLUTIONS

DANIEL SOLARTE FERRO

GRADUATION PROJECT SUBMITTED TO OBTAIN THE TITLE OF

CHEMICAL ENGINEER

ADVISORS:
JOSÉ ANTONIO LARA RAMOS, Chem. Eng., Ph.D.
FIDERMAN MACHUCA MARTÍNEZ, Chem. Eng., Ph.D.

UNIVERSITY OF VALLE
FACULTY OF ENGINEERING
SCHOOL OF CHEMICAL ENGINEERING
SANTIAGO DE CALI
2025

Effect of the TiO_2 Precursor Phase on the Synthesis of TiO_2-Black-Impregnated Electrodes in the Degradation of Acetaminophen Solutions

Daniel Solarte Ferro, José Antonio Lara Ramos, Fiderman Machuca Martínez

Escuela de Ingeniería Química, Universidad del valle, Santiago de Cali, Calle 13 # 100-00, CP 760032, Colombia

ABSTRACT

Black TiO_2 impregnated electrodes were synthesized using a modified dip-coating method with 6 layers, to account for the influence of the precursor phase (anatase, rutile, and P25), and their physical properties upon the response on photo electrooxidation of acetaminophen. The thermal treatment under $H_2 + Ar$ successfully narrowed the band gap and generated a formation of oxygen vacancies and Ti^{3+} species, confirmed through UV-Vis DRS and photoluminescence (PL) spectroscopy. Treated anatase phase exhibited the greatest band gap reduction, while rutile and P25 showed superior structural stability. The evaluation of acetaminophen degradation revealed a strong dependence on electrolyte medium; the process was ineffective on sulfate medium (Na_2SO_4, 0.1 *M*), but highly effective on chloride medium (NaCl, 0.1*M*). This analysis corroborated that dominant degradation pathway is indirect oxidation through electrogenerated active chlorine species. Rutile and P25 electrodes achieved the highest removal performance, with a minimum C/Co value of 0.631 and 0.650, respectively.

Keywords: Acetaminophen, Black TiO_2, Photo-electrooxidation, Emerging Contaminants, Precursor Phase, Dip-coating

1. Introduction

On recent years, there has been a growing concern regarding the presence of pollutants on wastewater, which led to the develop of advanced treatment methods capable of eliminate these emerging contaminants. Extremely sensitive techniques have revealed the presence of pharmaceuticals pollutants in aquatic environments, having extremely low concentrations and high health risks [1-4]. Specifically, acetaminophen has been studied due to its presence in global markets, making a continues release on domestic and industrial effluents [5-7]. However, conventional water treatments such as coagulation, adsorption, or filtration often present limitations on small concentrations, highlighting the need for other sustainable alternatives.

Among these alternatives, the advanced oxidation process (AOPs) has shown great relevance with its versatile tools for the degradation of organic pollutants [8-9]. In particular, photo electrooxidation combine UV irradiation with the application of electrical current, promoting the production of high oxidative species, capable of degrade a long range of compounds [10-11]. This method strongly depends on the nature of the anode material, which led to the development of materials, with good electronic properties to enhance the production of radicals and oxidative species [12].

Metal oxide semiconductors, such as zinc oxide (ZnO) and tin oxide (SnO_2), have been largely investigated for environmental remediation applications due to their electronic structure and catalytic capabilities [13-14]. Among these transition metal oxides, titanium dioxide (TiO_2) have demonstrated a competitive performance due to their chemical stability, low cost, and photocatalytic properties [15-18]. Black TiO_2 has enormous potential thanks to the narrowed band gap, defect-rich structure, and presence of oxygen vacancies [19-22]. But, considering that the photocatalytic and electrochemical performance is influenced by the crystalline precursor phase used in the synthesis, it is required to evaluate such factors to ensure the best performance on the degradation of pharmaceuticals pollutants.

The deposition method of catalytic material plays a crucial role in the stability, surface roughness, and availability of active sites. Several techniques have been employed, including spin coating and spray pyrolysis, each having different advantages with the impregnated film. However, dip coating stands-out, allowing a cheap, and versatile method, with a controlled and uniform coating layers, these

parameters can be easily replicable and controlled with the viscosity, immersed and withdrawn velocity [23-26]. Also, a key factor among the electrode coating, is the TiO_2 precursor phase on the formation of black TiO_2 and its behavior on photo electrooxidation degradation of pharmaceutical contaminants.

This work centers on evaluate the effectiveness of black TiO_2 coated electrodes, on the photo electrooxidation degradation of acetaminophen solution in chloride and sulfate media, researching the response of the precursor phase (anatase, rutile, P25 and anatase-rutile mixture) on the synthesis of black TiO_2 through hydrogen thermal treatment, and deposition on titanium electrodes, via dip coating. Characterizing these materials to understand the structural, morphological, and optical properties, also along with the degradation experiments, which were employed to correlate the physicochemical properties of the material with its activity.

2. Materials and methods

2.1 Materials

All the reagents were analytical grade and require no additional purification. For the Black TiO_2 synthesis, three precursors were used, commercial TiO_2 (P25 powder, Aeroxide), commercial anatase TiO_2 (Aldrich, 25 nm particle size, 99.7 % purity), and commercial rutile TiO_2 (powder, Sigma-Aldrich, < 5 micron particle size, 99.9 % purity). Additionally, commercial urea (CH_4N_2O, Supelco), for the solid state co-doping process. For the hydrothermal treatment, two atmospheres were employed, a gas mixture of hydrogen and argon (5.4 % H_2 + 94.6 % Ar, Messer), and N_2 gas (96 % purity).

Triton X-100 ($C_8H_{17}C_6H_4(OCH_2CH_2)_7nOH$, Sigma) as a surfactant for the electrode impregnation, commercial acetaminophen ($C_8H_9NO_2$) as a model compound for degradation tests, sodium chloride (NaCl, 99+ %, Aldrich), sodium sulfate (Na_2SO_4, Fisher Chemical) were used for electrolyte solutions.

2.2 Sample preparation

Four TiO_2 precursors were used in the synthesis, P25 powder, anatase nanopowder, and rutile powder. Another sample was prepared through chemical reaction of solid state, taking 20 % rutile and 80 % anatase phases. Additionally, a co-dopped process was conducted in a solid-state mixture with each initial sample, using a 20 % concentration of urea. All the prepared samples are presented in *Table 1.*

Table 1. *Summary of sample identification*

Sample	ID	Composition description
TiO_2 - P25	P25	Commercial P25 powder (mixed anatase/rutile)
TiO_2 - Rutile	R	Commercial rutile TiO_2 powder
TiO_2 - Anatase	A	Commercial anatase TiO_2 nanopowder
TiO_2 - Mix	M	Solid state mixture: 20% rutile / 80% anatase
TiO_2 - P25 + Urea	N, C P25	P25 sample co-doped with 20% urea (solid method)
TiO_2 - Rutile + Urea	N, C R	Rutile sample co-doped with 20% urea (solid method)
TiO_2 - Anatase + Urea	N, C A	Anatase sample co-doped with 20% urea (solid method)
TiO_2 - Mix + Urea	N, C M	Mix sample co-doped with 20% urea (solid method)

2.3 Black TiO_2 synthesis

For each precursor phase a hydrogen atmosphere thermal treatment was employed [19, 27-28]. All samples were placed on ceramic crucibles and introduced into a tubular furnace. The system was purged using N_2 gas for 15 minutes, followed by a calcination on H_2+Ar atmosphere with a flow rate of 10 sscm. The temperature was 800 °C, for 8 hours, with a heating and cooling rate of 10 °C/min. The obtained samples were stored and labeled with a similar identification as the untreated ones, except for the letter T before.

2.4 Characterization techniques

The characterization of pure, N, C solid state co-doped and thermally treated TiO_2 samples were conducted using scanning electron microscopy and energy-dispersive X-ray spectroscopy at 15 *kV* (SEM EDS, Phenom Pro X). UV–Vis DRS were recorded at room temperature using a UV–Vis spectrophotometer (V-770, Jasco) to excite the samples

within the working wavelength range of 200–1000 *nm* [22,29-30]. Kubelka–Munk function determined the optical band gap energy. Photoluminescence (PL) measurements were performed at room temperature using a spectrofluorometer (FP–8250, Jasco) in a range of 300-750 *nm* [29-30]. Fourier transform infrared (FTIR) measurements were also conducted using a spectrophotometer (FT/IR-6800, Jasco), and the spectra were recorded in the range of 4000–350 cm^{-1} [27,30]. Finally, the vibrational spectra were obtained using a Raman spectrometer (RMS 4500, Jasco) with a laser at 532 *nm*, in the range of 50–4000 cm^{-1} [30].

2.5 Electrode coating procedure

The black TiO_2 nanoparticles were dissolved in deionized water (Type I) with one drop of Triton X and concentration of 15 % w/v. Each solution was sonicated for 1 hour at 60 *kHz* to obtain a well particle dispersion.

Each electrode measured 2.0 × 2.5 *cm*, with a thickness of 5 *mm*, and were impregnated with dip-coating technique [23-24]. The electrodes were immersed in each black TiO_2 solution, with a controlled velocity of 10 *cm/min*, kept inside for 1 *min*, and withdrawn. Right after the coating, the electrodes were placed in a furnace with a heating ramp of 5 *°C/min* up to 150 *°C*, left there for 15 *min* for partial adhesion. Then, the electrodes were quenched in Type I water to remove any unattached particles and returned to the furnace for another 15 *min*, to repeat the coating process. This procedure was replicated until completing 6 coating layers. The deposited mass on each electrode was calculated from the difference between the non-coated electrode, and the coated one (equation (1).

$$m_d = m_f - m_i \quad (1)$$

were m_d is the deposited mass, m_f is the mass of the electrode after coating, and m_i is the initial mass of the uncoated electrode.

2.6 Photoelectric oxidation in the degradation of acetaminophen

The degradation of acetaminophen was carried out in a cell of two electrodes of 100 *mL*, using 0.1*M* NaCl (chloride medium) and 0.1*M* Na_2SO_4 (sulfate medium) [31-32]. The coated titanium electrodes (5 cm^2 geometric area), used as anode and cathode for the 90 *min* degradation test. A power supply was connected in series to a multiparameter meter to allow real-time measurement and control of the applied current, which was set to 12.5 *mA*, calculated based on a current density of 2.5 mA/cm^2, a magnetic stirring applied a 500 *rpm* to ensure optimal mass transport. The cell was placed inside a home-made photoreactor with a UV- visible lamp (main peaks measured at 436, 547, 405, 579, 399, and 313 *nm*) to excite the system during tests. The concentration analysis was performed by high performance liquid chromatographic (HPLC, Shimadzu LC-2010A HT series), using ODS2-SL5 column (5 μm, 4.6 × 250 *mm*), and mixture of a mobile phase, acetonitrile (Merck)- Type I, in a 40:60 proportion. The injection flow was 0.5 $mL \cdot min^{-1}$ and an ultraviolet detector at 243 *nm* [31,33-34].

3. Results and discussion

3.1 Structural and morphological analysis

Fig. 1 and 2 shows SEM images of TiO_2 samples and N, C co-doped TiO_2 samples and urea. The analysis confirmed that the precursors already have a well-defined sphere-like particle size distribution, except for the P25 phase, which exhibits an irregular and heterogeneous morphology, as typically reported for commercial powders [35-36]. After the N, C solid state co-doped process, all the samples presented a light increase in particle agglomeration, but the spherical shape of the particles remained on each phase, except for the P25 one, indicating that the co-doping process did not modify the morphology of the TiO_2 particles.

Energy-Dispersive X-ray Spectroscopy (EDS) was performed to obtain the elemental composition and atomic ratio of the samples, in the case of P25 sample, initially contains a higher molar concertation of carbon and oxygen more than anatase, rutile and mixed-phase samples, probably associated with the industrial synthesis process or organic residues [37]. However, after the N, C co-doping treatment, the atomic concentration of carbon increased across all samples, confirming the incorporation of species onto the surface. No nitrogen signal was observed in the co-doped samples. For the rest of the phases, oxygen was the predominating element before and after the co-doping process [38].

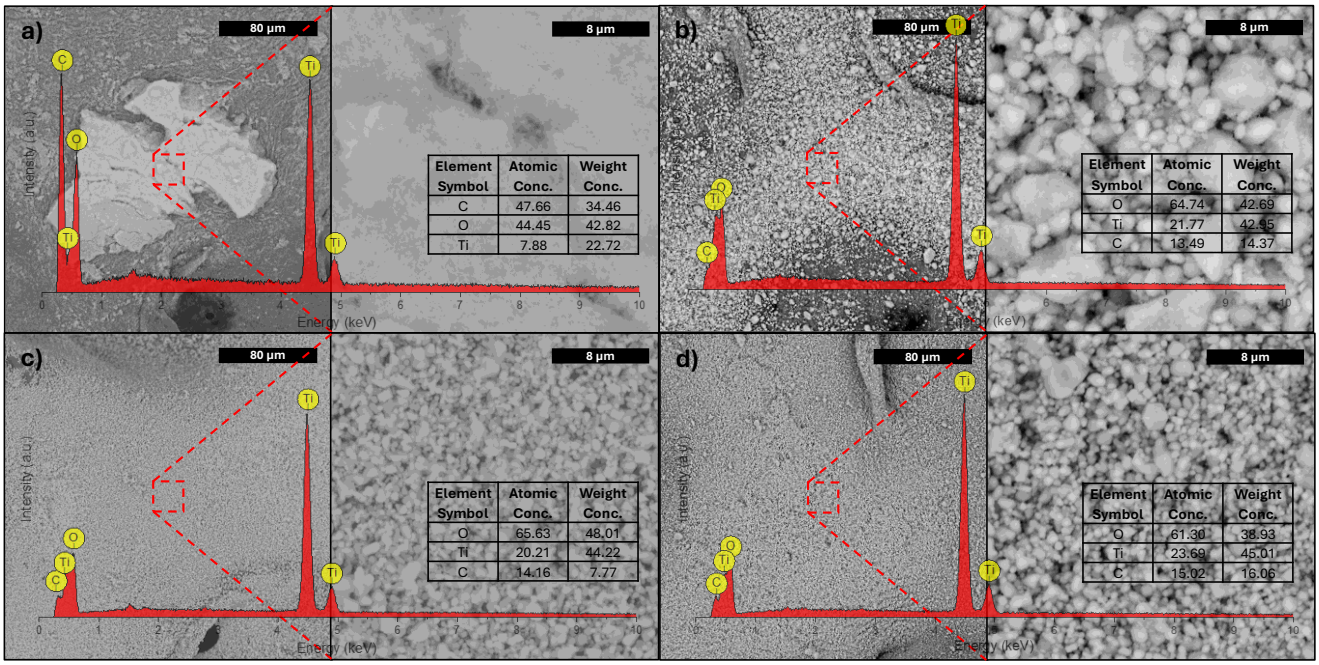

Fig. 1. *SEM images, and energy dispersive X-ray analysis of* TiO_2 *nanostructures: (a) P25, (b) Rutile, (c) Anatase, and (d) Mixture.*

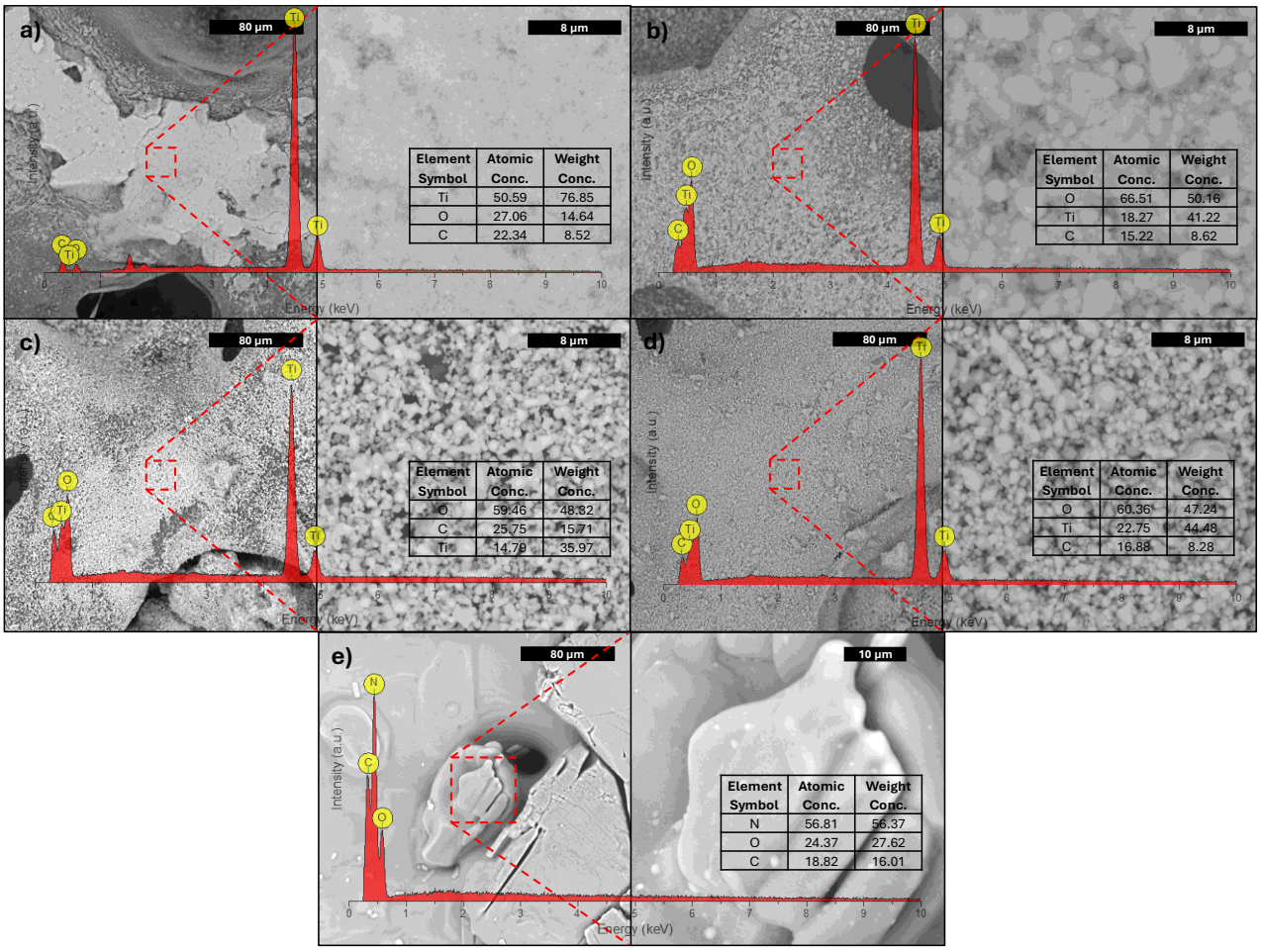

Fig. 2. *SEM images, and energy dispersive X-ray analysis of N,C co-doped TiO_2 nanostructures: (a) N,C P25, (b) N,C Rutile, (c) N,C Anatase, (d) N,C Mixture, and (e) Urea.*

3.2 Fourier transform infrared spectroscopy (FTIR)

The FTIR spectra in *Fig. 3* shows clearly, expected features of the TiO_2 samples. A set of bands around 465–477 cm^{-1} corresponds to the Ti–O and Ti–O–Ti stretching vibrations of the TiO_2 lattice, confirming the integrity of the oxide framework [39-41]. Broad absorptions near 3200–3400 cm^{-1} and a band around 1630 cm^{-1} are consistent with O–H stretching and bending, which indicates the presence of surface-adsorbed water or hydroxyl groups [42].

In the co-doped materials, new peaks appear at 1154, 1457, and 1622 cm^{-1}. These are best interpreted as C–N, C–O, and N–H vibrational modes, respectively, and provide direct spectroscopic evidence that nitrogen and carbon species were incorporated during synthesis. A weak band between 2320–2360 cm^{-1} is also observed and is assigned to the asymmetric stretch of adsorbed CO_2 [43].

After the thermal treatment all the signals associated with urea-derived organic groups (C–N, N–H, and C=O) largely disappear [44,50]. This loss of organic bands indicates that the urea dopant decomposed completely during thermal treatment, leaving the TiO_2 lattice bands as the dominant features. Minor contributions from CO_2 and surface hydroxyls remain, but the overall spectrum shows that the structural integrity of TiO_2 was preserved.

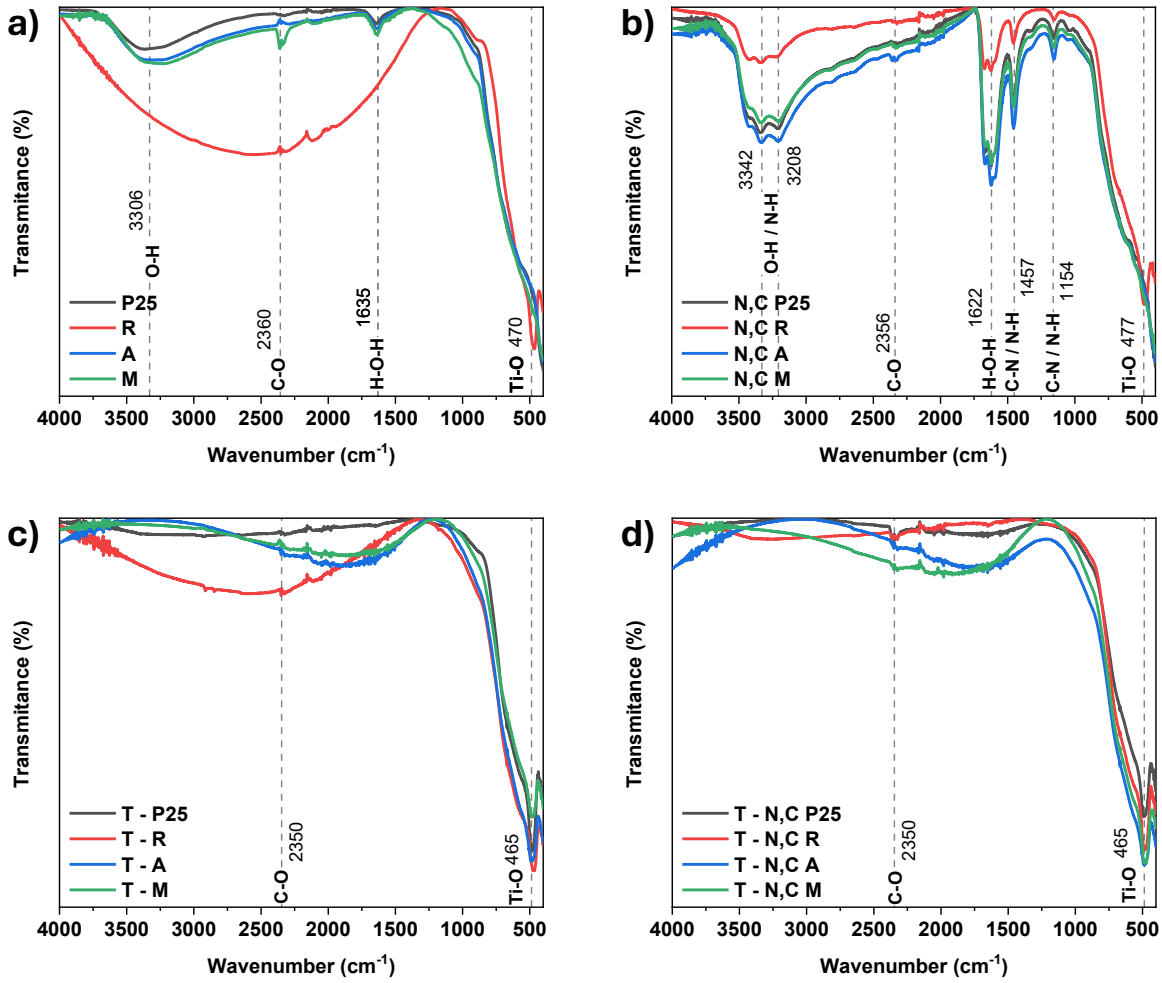

Fig. 3. *FTIR of TiO_2 samples: (a) pure TiO_2, (b) N,C co-doped TiO_2, (c) thermally treated pure TiO_2, and (d) thermally treated N,C co-doped TiO_2*

3.3 Raman spectroscopy

The Raman spectra shown in *Fig. 4* display the expected vibrational fingerprint of TiO_2, with bands at approximately 141, 189, 225, 390, 448, 511, and 634 cm^{-1} that correspond to the characteristic E_g, B_{1g} and A_{1g} modes of TiO_2 polymorphs. Mixed-phase samples (A, R, and M) present features attributable to both anatase and rutile, confirming their composite crystalline nature [37-38].

In the N, C co-doped materials, and alongside the Ti–O lattice vibrations, additional bands appear in the 1004–1010 cm^{-1} and 2700–3360 cm^{-1} regions [44-45]. These signals are consistent with residual organic moieties or vibrational modes introduced by N- and C-containing groups derived from the urea precursor, indicating partial retention of dopant-related functional groups in some samples [46].

After thermal treatment, the Raman spectra the N, C co-doped samples show a marked attenuation or complete loss of the bands associated with urea-derived species. This effect is most pronounced in the T–N, C A sample, which displays the cleanest spectrum and retains only the characteristic TiO_2 vibrational modes. These observations indicate that the thermal protocol effectively removes residual dopant-related organic fragments while preserving the crystallinity and structural integrity of the TiO_2 lattice [47].

The preservation of these modes across all treated samples demonstrates that the H_2 thermal process modifies the electronic structure (as shown in the band gap energy narrowing in UV-Vis), without modifying the crystalline structure [46]. This suggests that the defects produced are likely concentrated on the surface , creating active sites while maintaining structural stability for the electrode application.

3.4 Optical properties of TiO_2 (UV-Vis spectroscopy)

Fig. 5 shows the UV–Vis diffuse reflectance spectra (UV–Vis DRS) of pure, urea co-doped, and thermally treated TiO_2 samples. UV–Vis DRS was employed to determine the band gap energy of the materials using the Kubelka–Munk function, *F(R)*, which is related to the diffuse reflectance (equation (2) [36,41].

$$F(R) = \frac{(1-R)^2}{2R} \quad (2)$$

The energy values of the nanostructures were calculated by plotting $[F(R)hv]^{1/2}$ vs. photon energy (hv), where h is Planck's constant and v is the photon frequency [38,40-42]. In the linear region of the function, a straight line was extrapolated to calculate de indirect band gap as $E_g = -b/m$, where b and m are the intercept and slope of the linear fit.

The uncertainty was derived by propagation from standard errors of the fit parameters. The same procedure was performed to calculate the direct band gap energy, by modifying the function to $[F(R)hv]^2$, as shown in *Fig. 6.* The obtained direct and indirect band gap energies were summarized in *Table 2*.

The UV-Vis DRS of *Fig. 4* shows a clear decrease in reflectance intensity for the pure and N, C co-doped TiO_2 treated samples compared to the nontreated ones. This behavior suggests an enhancement in light abortion, due to the formation of defect-related states and dopant-induced energy levels [43-44]. In general, the pure TiO_2 samples exhibit typical values close to 3.3 *eV* (direct) and 3.0 *eV* (indirect), as shown in *Fig. 5*, consistent with the literature for anatase- and rutile-type TiO_2. A slight reduction in band gap energy was observed for the N, C co-doped samples, suggesting the introduction of dopant-induced states within the band structure.

After thermal treatment under a $H_2 + Ar$ reducing atmosphere, all samples exhibited a significant narrowing of both direct and indirect band gaps. This effect is particularly pronounced in the treated anatase sample (2.97 *eV* direct, 2.64 *eV* indirect), indicating the formation of oxygen vacancies and Ti^{3+} centers [47-50]. The combination of dopant atoms and reduction treatment therefore promotes the creation of localized mid-gap states, which extend the optical absorption of TiO_2 toward the visible region and may enhance its photoactivity.

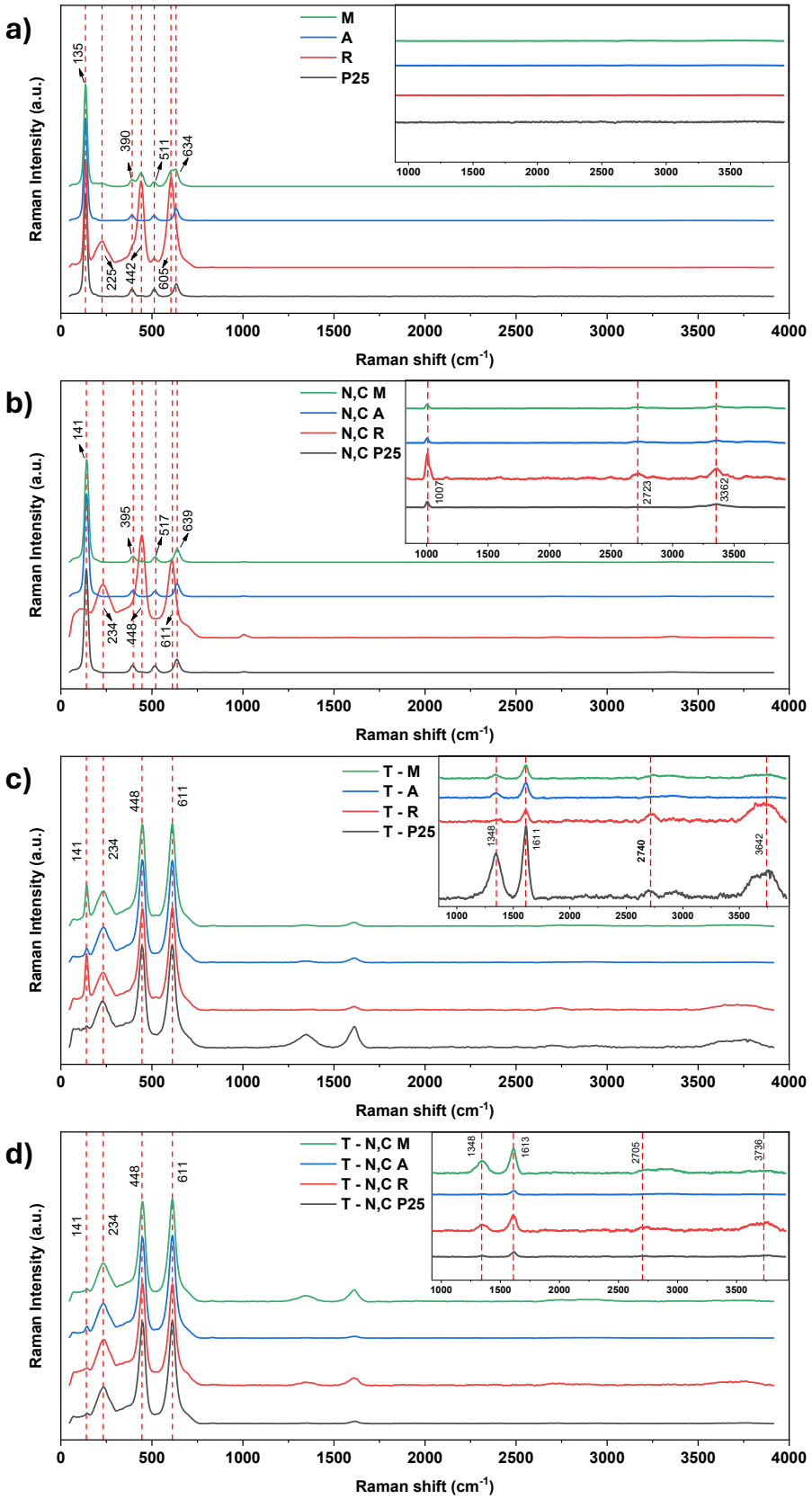

Fig. 4. *Raman spectra of : (a) pure TiO_2, (b) N,C solid state co-doped TiO_2, (c) thermally treated pure TiO_2, and (d) thermally treated N,C co-doped TiO_2.*

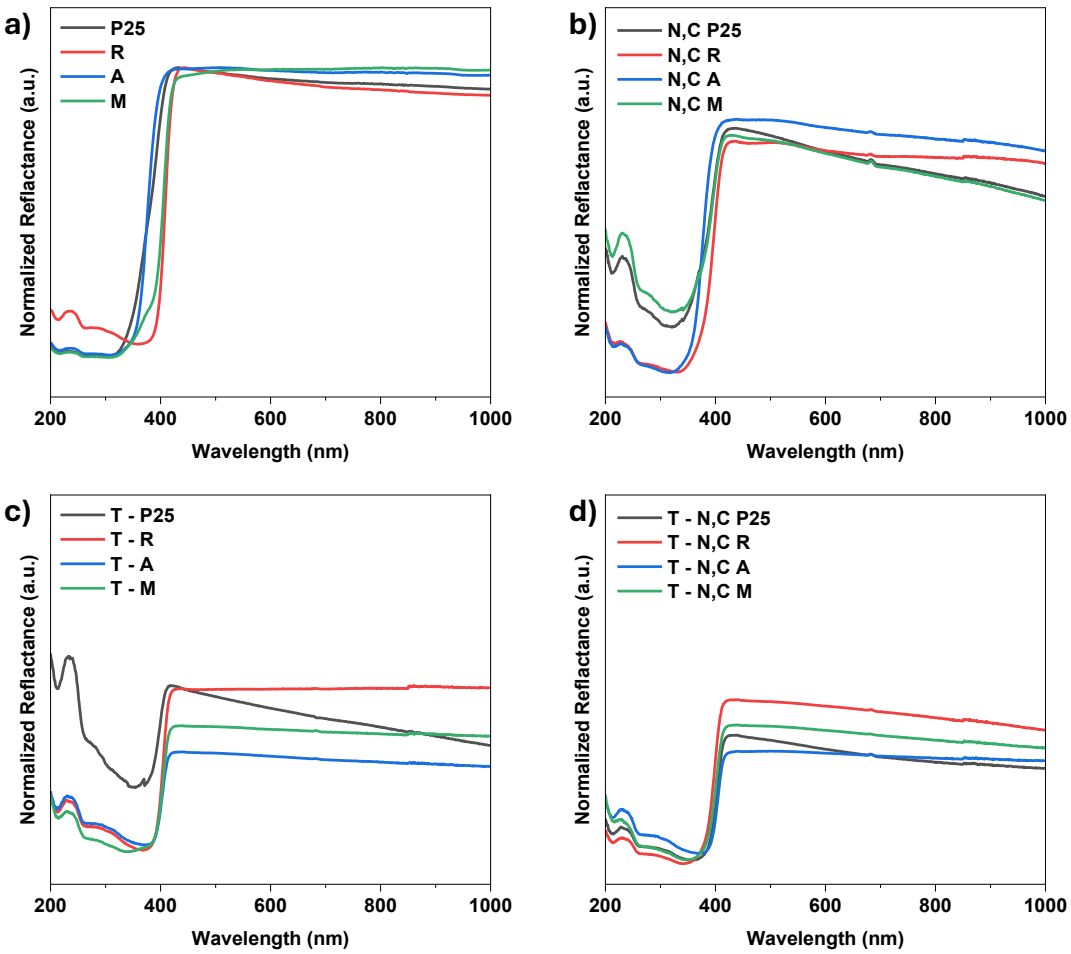

Fig. 5. *UV-Vis DRS of TiO_2 samples: (a) pure TiO_2, (b) N,C co-doped TiO_2, (c) thermally treated pure TiO_2, and (d) thermally treated N,C co-doped TiO_2.*

3.5 Photoluminescence spectroscopy

Fig. 7 shows the photoluminescence spectra (PL) of all TiO_2 samples. The results served as direct confirmation of the defect states previously inferred from the UV-Vis DRS analysis. Since the spectral data were normalized, an intensity ratio analysis was performed relative to a reference point to precisely compare the variation of each emission peak. The samples exhibited a consistent emission bands, according to the literature [47,50]. The pure samples exhibited peak intensity in central emission region (399 – 469 *nm*), attributed to oxygen vacancies and sub- band gap defect states, associated with Ti^{3+}-related mid-gap levels.

The introduction of N, C dopants reorganized the PL intensity distribution, the central region intensified along all phases, showing the formation of new defects sites, such as oxygen vacancies [49]. Rutile lost its dominant peak, suggesting that dopants introduce non-radiative pathways that redistribute charge carriers. Also, P25 lost its emission on 397 *nm*, implying improved charge separation or a modification of electronic states at the phase interface.

After the thermal treatment, induced drastic spectral shifts, by the reduction conditions of the procedure. P25 sample got the most radical change, developing a sharp increase on the 320 *nm* peak, overshadowing all the central emission. This peak corresponds from defect states introduced by oxygen vacancies, reduced Ti sites, or treatment in reducing atmospheres [43]. The anatase and mixed-phase samples largely mirrored the initial rutile spectrum, indicating that the rutile is less sensitive to defect redistribution, partially thanks to its lack of phase transition.

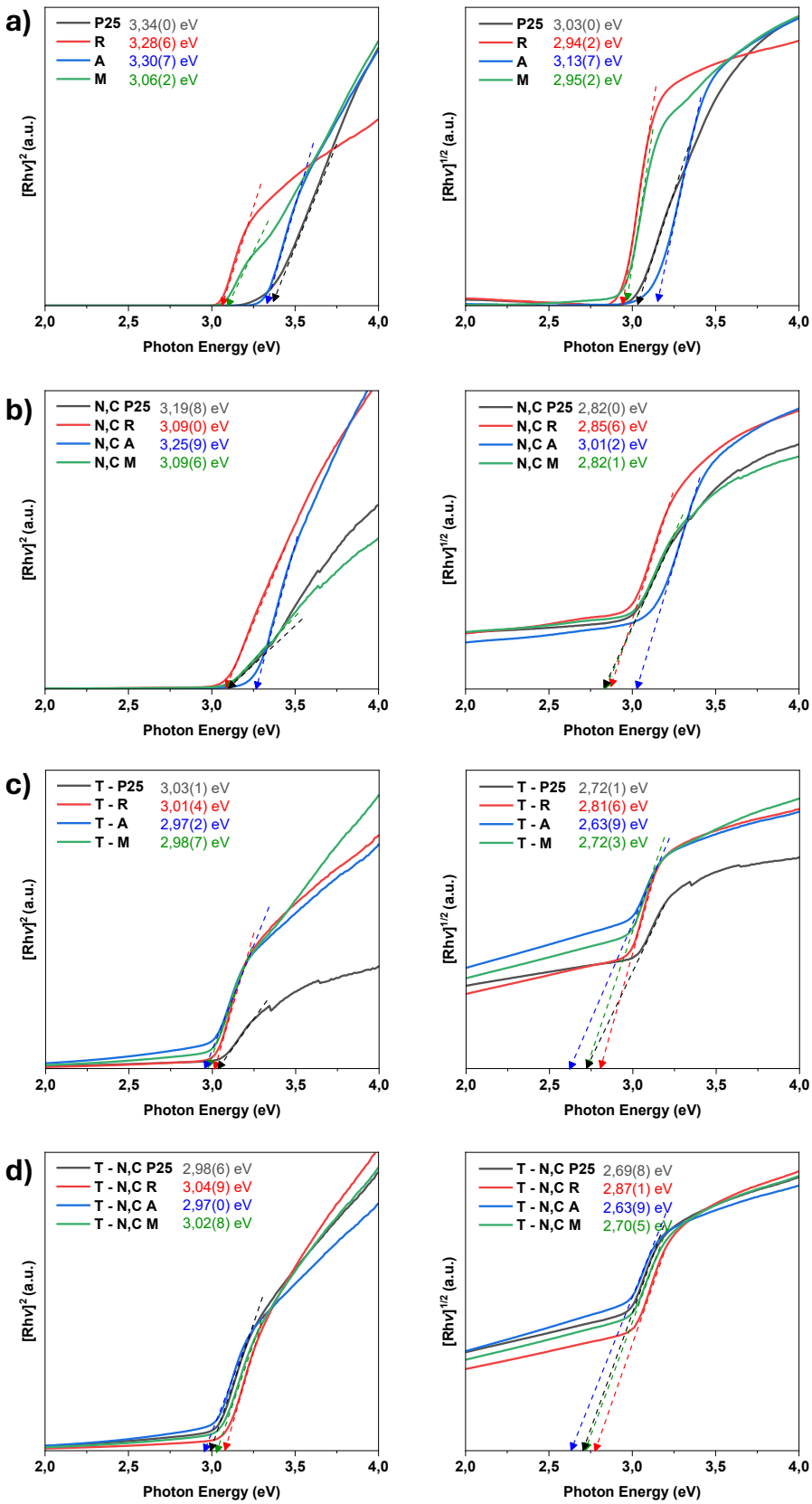

Fig. 6. *Tauc's plots obtained by the Kubelka–Munk method for direct and indirect transition: (a) pure TiO_2 samples, (b) of N, C solid state co-doped TiO_2, (c) pure treated TiO_2 samples, and (d) treated N,C solid state co-doped TiO_2.*

Table 2. *Band gap energies of pure, N,C co-doped, and treated TiO_2 samples obtained from UV-VIS DRS.*

Sample ID	Band Gap Energy (eV)	
	Direct	Indirect
P25	3.340 ± 0.030	3.030 ± 0.027
R	3.286 ± 0.029	2.942 ± 0.026
A	3.307 ± 0.029	3.137 ± 0.028
M	3.062 ± 0.027	2.952 ± 0.026
N, C P25	3.198 ± 0.028	2.820 ± 0.025
N, C R	3.090 ± 0.027	2.856 ± 0.025
N, C A	3.259 ± 0.029	3.012 ± 0.027
N, C M	3.096 ± 0.027	2.821 ± 0.025
T - P25	3.031 ± 0.027	2.721 ± 0.024
T - R	3.014 ± 0.027	2.816 ± 0.025
T - A	2.972 ± 0.026	2.639 ± 0.023
T - M	2.987 ± 0.026	2.723 ± 0.024
T - N, C P25	2.986 ± 0.026	2.698 ± 0.024
T - N, C R	3.049 ± 0.027	2.871 ± 0.025
T - N, C A	2.970 ± 0.026	2.639 ± 0.023
T - N, C M	3.028 ± 0.027	2.705 ± 0.024

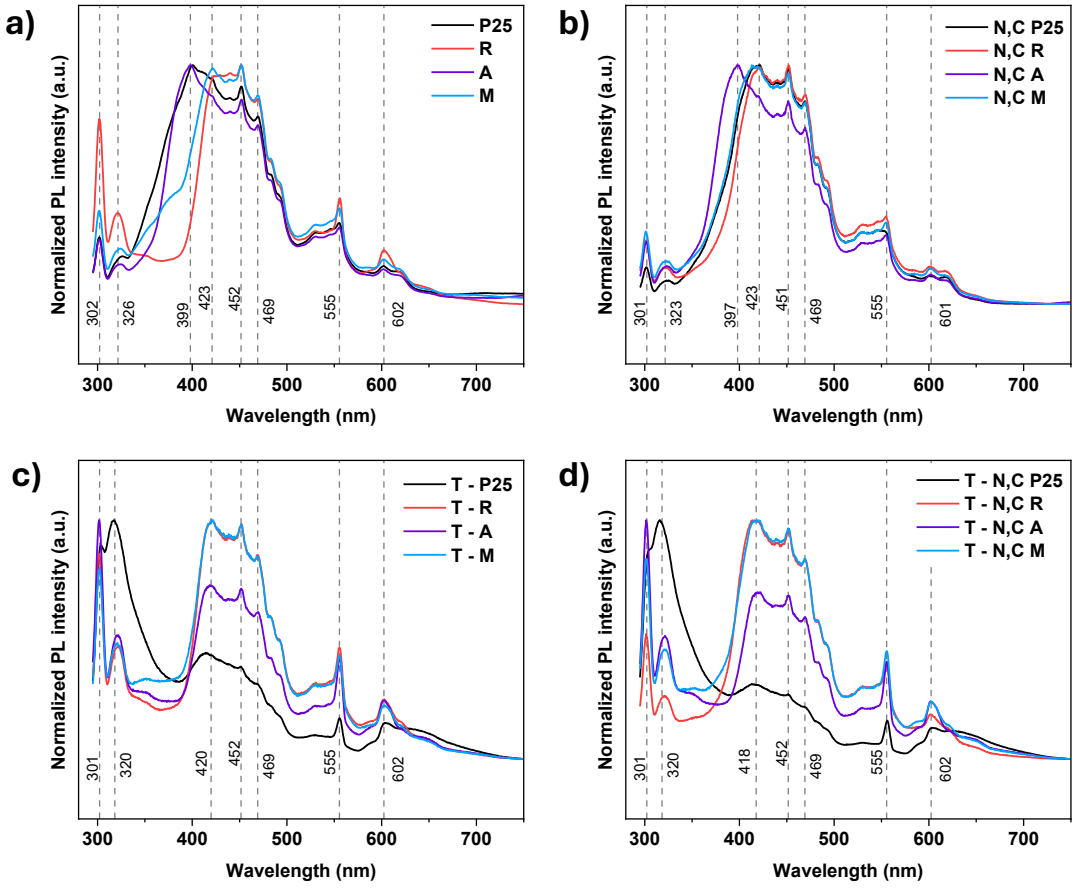

Fig. 7. *PL spectra of TiO_2 samples: (a) pure TiO_2, (b) N,C co-doped TiO_2, (c) thermally treated pure TiO_2, and (d) thermally treated N,C co-doped TiO_2.*

Finally, the co-doped thermally treated samples followed the trends of the pure treated samples, confirming that the reducing treatment is the dominant factor in defect formation. However, a clear difference can be seen, rutile exhibited a significant drop in intensity at both 302 and 320 *nm*, suggesting that the presence of dopants helps passivate or redistribute the deep-level defects created during reduction [49-50].

3.6 Deposition of black TiO_2 on electrodes.

The deposition of black TiO_2 onto the titanium sheets substrate, using controlled dip coating technique was successfully archive. A six-layer configuration avoided excessive material accumulation, for the mechanical stability of each electrode. The quench processes have proven effective to remove any loose particles and promote tighter packing among the surface. As a result, the final coating shows good uniformity and adhesion. Table 3 summarizes the mass deposited on the anode and cathode for each precursor phase. The black TiO_2 anatase coating layer produced the highest deposited mass, with 0.0041g on the anode and 0.0043g on the cathode, suggesting stronger particle-substrate interaction and a nicer dispersion during the coating process. On the other hand, rutile coated electrode shows the lowest deposited mass, likely due to its larger particle size and lower surface area, which can lead to limiting the adhesion of each layer.

Table 3. *Deposited mass of each electrode.*

Sample (TiO_2 phase)	Anode mass (g)	Cathode mass (g)
Black TiO_2 (P25)	0.0037 ± 0.000141	0.0034 ± 0.000141
Black TiO_2 (Rutile)	0.0029 ± 0.000141	0.0031 ± 0.000141
Black TiO_2 (Anatase)	0.0041 ± 0.000141	0.0043 ± 0.000141
Black TiO_2 (Mix)	0.0034 ± 0.000141	0.0037 ± 0.000141

3.7 Photo electrooxidation for the degradation of acetaminophen

The photo electrooxidation to remove the acetaminophen was performed to compare the performance of black TiO_2-coated electrodes with each precursor phases and non-coated one. Overall, the experiment yields negligible degradation in sulfate medium (0.1M Na_2SO_4) across all the electrodes, with exception of the mixed-phase one, which achieved a final C/C_0 value of 0.926, although it maintained concentrations above 0.976 throughout most of the assay (*Fig. 8*) [31]. On the other hand, the experiments performed on the chloride medium (NaCl), exhibited significantly higher conversion rates. The most effective performances were observed for Rutile and P25 precursor phases, which reached minimum C/C_0 values of 0.631 and 0.650, respectively.

Comparing the results against the non-coated electrodes, which achieved a C/C_0 of 0.850, the enhance of the degradation of acetaminophen, provided by the impregnation process, appears moderate. The total difference between the coated and non-coated electrodes is pronounced, suggesting that, under this specific set of experimental conditions, the coating contributes to the degradation, but does not exponentially amplify it over time.

The results indicate that the degradation mechanism got dominated by indirect oxidation via electrogenerated active chlorine species, (such as $HOCl, Cl_2, OCl^-$)[P]. In the presence of NaCl electrolyte, anodic electrolysis promoted the formation of these highly reactive species [31,51]. Along the photocatalysis, the concentration of these agents increased, been capable of oxidizing and mineralizing acetaminophen. This cumulative process explains the performance over longer duration on each experiment. In contrast, on the Na_2SO_4 medium, the absence of these species precludes this indirect pathway, obtaining a limited degradation [51]. The slight activity observed on the mixed-phase electrode can be explained by a partially direct oxidation process.

During the HPLC monitoring, two distinct additional signals were detected in chromatograms at different retention times from the acetaminophen. Although these sub-products were not quantified in this study, their appearance confirms the stepwise degradation of acetaminophen, due to the attack of chlorine species [31].

An analysis of variance (ANOVA) was conducted to quantify the impact of the experimental conditions on the degradation efficiency of acetaminophen. The results of *Table 4* confirm that the electrolyte composition is the governing factor in the system, with a value of $p = 1.52e\text{-}07$, outweighing the influence of precursor phase, during the coating process. These statistical results aligned with the experimental behavior, along the generation of chlorine species, capable of degradation the acetaminophen.

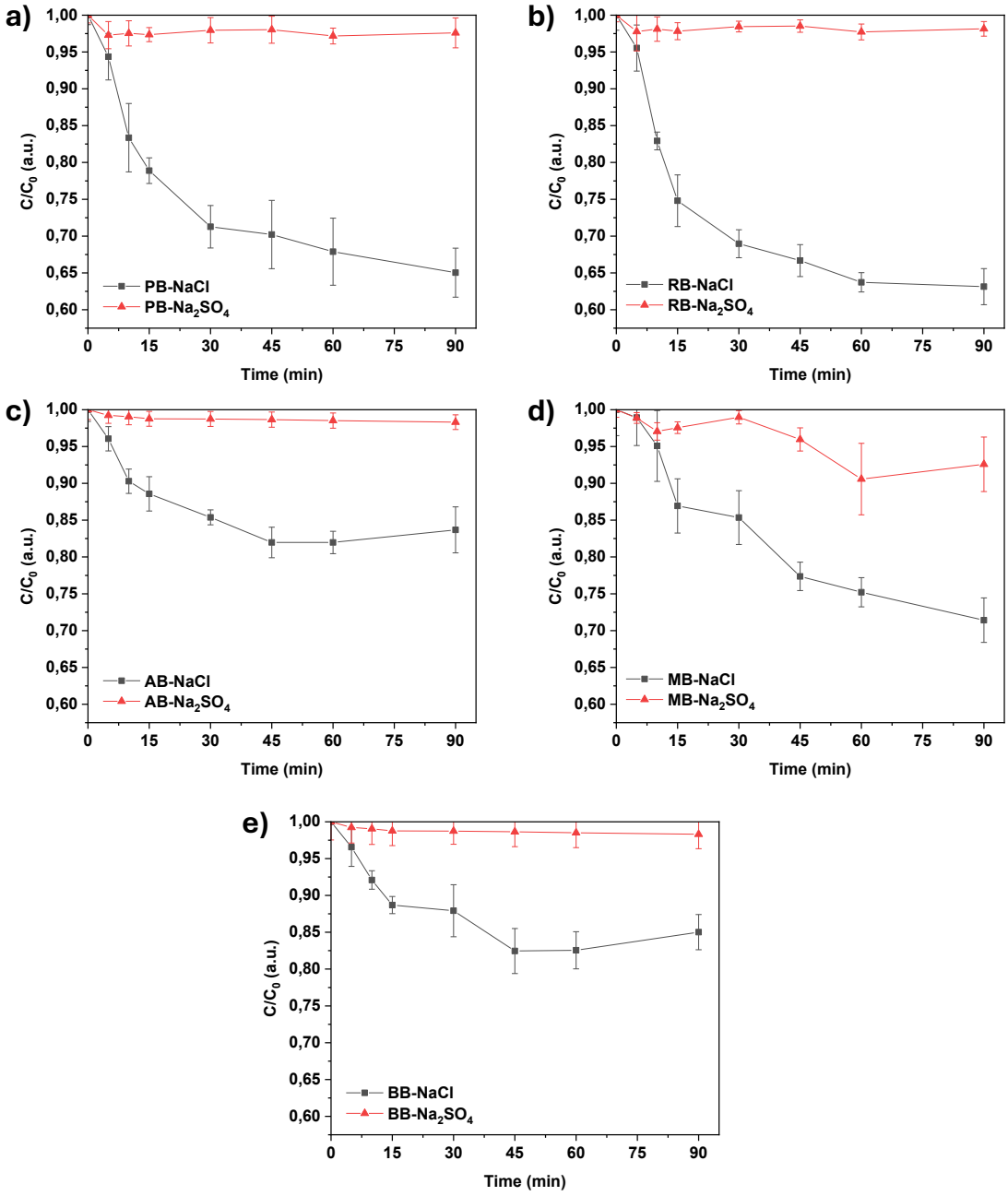

Fig. 8. *Degradation profiles of acetaminophen on 0.1 M NaCl and 0.1 M Na_2SO_4 electrolytes, (a) black P25, (b) black rutile, (c) black anatase, (d) black anatase-rutile mixture, and (e) non-impregnated electrode.*

However, the precursor type also exhibited a significant effect ($p = 9.65e\text{-}03$). Indicating that the precursor selected during the black titania synthesis does contribute to measurable degradation difference, due to their unique set of properties previously measured.

Fig. 9 show the interaction plot, confirming the primary driving factor on the photo electrooxidation degradation is the electrolyte composition. Along all the electrode precursors, the average degradation achieved on NaCl medium is substantially higher than the Na_2SO_4 medium, the difference is consistent with the statistical significance on ANOVA. In Na_2SO_4 medium, degradation values remain uniformly low and largely indistinguishable from each other. But, in NaCl medium, the rutile and P25 coated precursors (RB and PB), exhibit the highest degradation efficiency, in contrast with the lowest response, the uncoated electrode (BB).

Table 4. *ANOVA for the effects of electrolyte and precursor type on acetaminophen degradation.*

Source of Variation	Sum of Squares (sum_sq)	Degrees of Freedom (df)	F-value (F)	p-value (PR(>F))
C(Electrolyte)	0.285560	1.0	165.37	1.52e-07
C(Precursor)	0.041845	4.0	6.058	9.65e-03
C(Precursor):C(Electrolyte)	0.035761	4.0	5.177	1.60e-02
Residual	0.017268	10.0	NaN	NaN

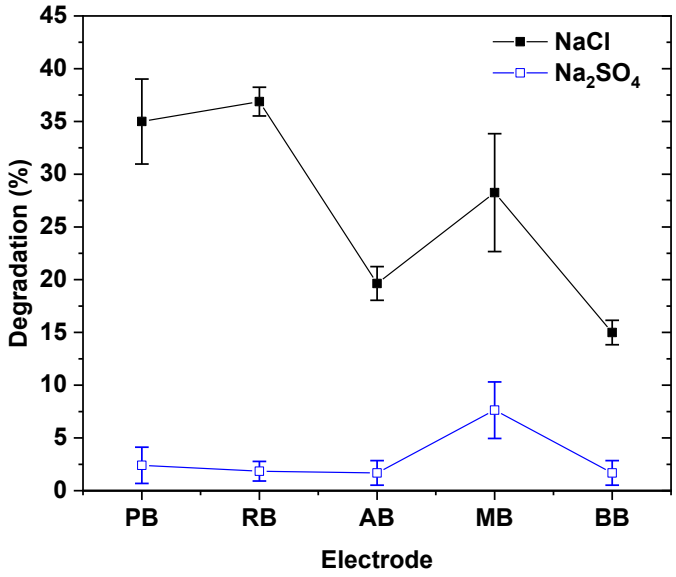

Fig. 9. *ANOVA interaction plot for precursor and electrolyte factors.*

4. Conclusions

The synthesis of black TiO_2 nanostructures were satisfactorily achieved using various crystalline precursors (P25, anatase, rutile, and a mixture). The thermal treatment with the hydrogen atmosphere proven to be the most crucial step, significantly narrowing the band gap energy, across all the samples, enhancing the visible light absorption. The anatase phase shows the most significant reduction in band gap energy due to the formation of oxygen vacancies and Ti^{3+} centers, while rutile and P25 demonstrated a stronger optical stability.

The dip coating technique successfully produced a uniformed film on each electrode with a six-layer configuration. The interaction between the catalytic powder and the substrate varied on each phase, anatase yielded the highest deposited mass, suggesting a superior adhesion property, meanwhile, the rutile phase obtained the lowest deposited mass, likely doe to its particle size and lower surface area.

The photo electrooxidation performance, revealed that the reaction medium plays a critical role in the degradation efficiency of acetaminophen. On the sulfate medium, the degradation was negligible, but highly effective in chloride medium. Confirming that the degradation is carried out in the indirect oxidation mechanism, by the production of active chlorine species (HOCl and OCl^-). Notably, while the anatase got the best coating, the electrodes based on rutile and P25 achieved the highest contaminate removal rates on chloride medium.

Declaration of competing interest

The authors declare that they have no known competing financial interests or personal relationships that could have appeared to influence the work reported in this paper.

References

[1] Adeola, A. O., Paramo, L., Fuoco, G., & Naccache, R. (2024). *Emerging hazardous chemicals and biological pollutants in Canadian aquatic systems and remediation approaches: A comprehensive status report. Science of The*

Total Environment. https://doi.org/10.1016/j.scitotenv.2024.176267

[2] Hernández-Tenorio, R., Guzmán-Mar, J. L., & Hinojosa-Reyes, L. (2022). *A review of occurrence of pharmaceuticals worldwide for environmental water matrices. Science of the Total Environment.* https://doi.org/10.1016/j.scitotenv.2022.158302

[3] Wu, J.-L., Liu, Z., Dai, L., & Dang, Z. (2023). *Occurrence, removal and risk evaluation of ibuprofen and acetaminophen in municipal wastewater treatment plants: A critical review. Science of The Total Environment, 891*, 164600. https://doi.org/10.1016/j.scitotenv.2023.164600

[4] Wada, O. Z., & Olawade, D. B. (2025). *Recent occurrence of pharmaceuticals in freshwater: global trends, contamination pathways, and treatment technologies. Chemosphere.* https://doi.org/10.1016/j.chemosphere.2025.144153

[5] Muambo, K. E. et al. (2024). *Pharmaceuticals in raw and treated water from drinking-water sources: occurrence, treatment, and risk assessment. Water Research.* https://doi.org/10.1016/j.watres.2024.121112

[6] Díaz-Moreno, C., & Rodríguez-Demaris, J. (2023). *Occurrence, removal and risk evaluation of ibuprofen and acetaminophen in municipal wastewater treatment plants: A critical review. Science of the Total Environment, 891*, 164600. https://doi.org/10.1016/j.scitotenv.2023.164600

[7] Wu, J., et al. (2025). *Environmental risk assessment of paracetamol in aquatic ecosystems using species sensitivity distribution and global occurrence data. Journal of Hazardous Materials, 499*, 140107. https://doi.org/10.1016/j.jhazmat.2025.140107

[8] Feijoo, S., Yu, X., Kamali, M., Appels, L., & Dewil, R. (2023). *Generation of oxidative radicals by advanced oxidation processes (AOPs) in wastewater treatment: a mechanistic, environmental and economic review. Reviews in Environmental Science and Bio/Technology, 22*(1), 205-248. https://doi.org/10.1007/s11157-023-09645-4

[9] Dewil, R., Appels, L., & Kamali, M. (2020). *Advanced oxidation processes for wastewater treatment: A review of recent trends, mechanisms and applications.* Journal of Environmental Chemical Engineering, 8(5), 104364. https://doi.org/10.1016/j.jece.2020.104364

[10] Garcia-Segura, S., Lanzarini-Lopes, M., Hristovski, K., & Westerhoff, P. (2020). *Electrocatalytic treatment of organic contaminants in water: A review of electrode materials and reaction pathways. Applied Catalysis B: Environmental, 270*, 118857. https://doi.org/10.1016/j.apcatb.2020.118857

[11] Busra Kus, Mesut Sezer, Melike Isgoren, Sevil Veli. (2025). *Anodic electrooxidation of textile wastewater by using spray coating Ti/TiO_2–RuO_2–IrO_2 anode: Response surface optimization of the process.* Journal of the Indian Chemical Society, 102, 101595. https://doi.org/10.1016/j.jwpe.2021.102568

[12] Fengxia Long, Danyal Ghani, Rongfu Huang, Chuntian Zhao. (2025). *Versatile electrode materials applied in the electrochemical advanced oxidation processes for wastewater treatment: A systematic review.* Separation and Purification Technology, 345, 128725. https://doi.org/10.1016/j.seppur.2024.128725

[13] Kim Hoong Ng, Kaijuan Chen, Chin Kui Cheng, Dai-Viet N. Vo. (2021). *Elimination of energy-consuming mechanical stirring: Development of auto-suspending ZnO-based photocatalyst for organic wastewater treatment.* Journal of Hazardous Materials, 409, 124532. https://doi.org/10.1016/j.jhazmat.2020.124532

[14] Imam Hussain, Ayesha Bibi, M. Imad Khan Khail, Tong Zhenbo, Rashid Khan, Zahid Hussain, Fu-Gen Yu, Chen Zao Zao, M. Kamran Khan. (2025). *Advancing environmental remediation: Mechanistic insights into SnO_2-based photocatalysts for organic pollutant degradation and microbial inactivation.* Journal of Water Process Engineering, 77, 108511. https://doi.org/10.1016/j.jwpe.2025.108511

[15] Laura Isabel Castaño, Gloria María Doria Herrera. (2020) *Revisión sistemática del proceso de degradación de contaminantes orgánicos persistentes en aguas residuales, provenientes de la industria farmacéutica por fotocatálisis heterogénea.* https://repository.unad.edu.co/handle/10596/36791

[16] Hong, D., Jiang, J., Lu, X., Yang, X., Jing, X., Zhong, F., Luo, S., Wang, Y., Wang, Y., Wang, F., Li, W., & Liu, G. (2026). *Synergistic enhancement of visible-light photocatalysis in TiO_2 microspheres via co-modification with CuS nanoparticles and black phosphorus quantum dots.* Material Today, 50, 114363. https://doi.org/10.1016/j.mtcomm.2025.114363

[17] Marta Jaruga, Michał Cegłowski, Adam Kubiak. (2025). *Unraveling the role of sponge matrix in the design of a 3D nature-inspired TiO_2-based photocatalyst for ketoprofen removal from wastewater.* Applied Surface Science Advances, 30, 100858. https://doi.org/10.1016/j.apsadv.2025.100858

[18] Erkan Cakiroglu, Suleyman Demir, Erdal Celik. (2025). *Detoxification of wastewater with toxic cyanide substance using TiO_2-based photocatalysts.* Environmental Nanotechnology, Monitoring & Management, 24, 101087. https://doi.org/10.1016/j.enmm.2025.101087

[19] Xuelan Hou, Yiyang Li, Hang Zhang, Peter D. Lund, James Kwan and Shik Chi Edman Tsang. (2024). *Black titanium oxide: synthesis, modification, characterization, physiochemical properties, and emerging applications for energy conversion and storage, and environmental sustainability.* Chemical Society Reviews, 53, 10660.

https://pubs.rsc.org/en/content/articlelanding/2024/cs/d4cs00420

[20] Hugo Olvera-Vargas, Oscar Andrés Jaramillo-Quintero, Luis Darío Alarcón León, Orlando Castro-Ocampo, Christian A. Celaya, Marina E. Rincón, Jesús Muñiz. (2025). *Green synthesis of glycolic acid through the electrocatalytic reduction of oxalic acid over black TiO_2: An experimental and theoretical study.* Journal of Energy Chemistry, 100, 544-556. https://doi.org/10.1016/j.jechem.2024.09.011

[21] Soontorn Tuntithavornwat, Chonticha Saisawang, Thanchanok Ratvijitvech, Anyarat Watthanaphanit, Mali Hunsom, Arunachala M. Kannan. (2024). *Recent development of black TiO_2 nanoparticles for photocatalytic H_2 production: An extensive review.* International Journal of Hydrogen Energy, 55, 1559-1593. https://doi.org/10.1016/j.ijhydene.2023.12.102

[22] Manjunath Veeranna Shinnur, MariaPia Pedeferri, Maria Vittoria Diamanti. (2024). *Properties and photocatalytic applications of black TiO_2 produced by thermal or plasma hydrogenation.* Current Research in Green and Sustainable Chemistry, 8, 100415. https://doi.org/10.1016/j.crgsc.2024.100415

[23] Munirathinam Elavarasan, Kasimayan Uma, Thomas C.K. Yang. (2020). *Photocatalytic oxidation of ethanol using ultrasonic modified TiO_2; an in-situ diffuse reflectance infrared spectroscopy study.* Results in Physics, 13, 102237. https://doi.org/10.1016/j.rinp.2019.102237

[24] F. Abbas, R. Bensaha, H. Taroré. (2020). *The influence of Zn^{+2} doping and annealing temperature on grown-up of nanostructures TiO_2 thin films prepared by sol-gel dip-coating method and their photocatalytic application.* Optik, 180, 361-369. https://doi.org/10.1016/j.ijleo.2018.11.020

[25] Chalita Mungsuk, Suriyakit Yommee, Sitthisuntorn Supothina, Paradee Chuaybamroong. (2023). *Solar photocatalytic degradation of carbendazim in water using TiO_2 particle- and sol-gel dip-coating filters.* Results in Engineering, 19, 101348. https://doi.org/10.1016/j.rineng.2023.101348

[26] Mathana Wongaree, Adisak Bootwong, Yingyote Lubphoo, Rattabal Khunphonoi. (2022). *Evaluation of wastewater treatment using CNT/TiO2 coating on a glass slide by a dip-coating method.* Desalination and Water Treatment, 245, 217-225. https://doi.org/10.5004/dwt.2022.27983

[27] T.S. Rajaraman, Sachin P. Parikh, Vimal G. Gandhi. (2020). *Black TiO_2: A review of its properties and conflicting trends*. Chemical Engineering Journal, 389, 123918. https://doi.org/10.1016/j.cej.2019.123918

[28] Luminita Andronic and Alexandru Enesca. (2020). *Black TiO2 Synthesis by Chemical Reduction Methods for Photocatalysis Applications.* Frontiers in Chemistry, 8. https://doi.org/10.3389/fchem.2020.565489

[29] Lei Zhang, Tze Chiang Albert Ng, Ximeng Liu, Qilin Gu, Yajun Pang, Zhixiao Zhang a, Zhiyang Lyu, Zeming He, How Yong Ng, John Wang. (2020). *Hydrogenated TiO2 membrane with photocatalytically enhanced anti-fouling for ultrafiltration of surface water.* Applied Catalysis B: Environmental, 264, 118528. https://doi.org/10.1016/j.apcatb.2019.118528

[30] Munirathinam Elavarasan, Kasimayan Uma, Thomas C.K. Yang. (2020*). Photocatalytic oxidation of ethanol using ultrasonic modified TiO2; an in-situ diffuse reflectance infrared spectroscopy study*. Results in Physics, 13, 102237. https://doi.org/10.1016/j.rinp.2019.102237

[31] Juan M. Sterling-Montealegre, Luis Norberto Benitez, Ricardo E. Palma-Goyes, Rosa M. Luna-Sanchez, Franklin Ferraro, Roberto L. Palomino-Resendiz, Selene M. García-Solares, Jorge Vazquez-Arenas. (2024). *Unraveling the influence of deposited layers on Ti/RuO2 anodes to define the electroactivity of oxygen evolution and active chlorine reactions.* Journal of Electroanalytical Chemistry, 973, 118645. https://doi.org/10.1016/j.jelechem.2024.118645

[32] Subburaj Srinithi, Vellaichamy Balakumar, Shen-Ming Chen. (2022). *In-situ fabrication of polypyrrole composite with MoO_3: An effective interfacial charge transfers and electrode materials for degradation and determination of acetaminophen*. Chemosphere, 291, 132977. https://doi.org/10.1016/j.chemosphere.2021.132977

[33] Miguel Angel Lopez Zavala, Camila Renee Jaber Lara. (2020). *Degradation of Paracetamol and Its Oxidation Products in Surface Water by Electrochemical Oxidation*. Environmental Engineering Science, 35. https://doi.org/10.1089/ees.2018.0023

[34] Miguel Ángel López Zavala, Diego Anglés Vega, José Manuel Álvarez Vega, Odwer Francisco Castillo Jerez, Rodrigo Alejandro Cantú Hernández. (2020). *Electrochemical oxidation of acetaminophen and its transformation products in surface water: effect of pH and current density*. Heliyon, 6, e03394. https://doi.org/10.1016/j.heliyon.2020.e03394

[35] Najoua Bouzakher-Ghomrasni, Olivier Taché, Jocelyne Leroy, Nicolas Feltin, Fabienne Testard, Carine Chivas-Joly. (2021). *Dimensional measurement of TiO_2 (Nano) particles by SAXS and SEM in powder form.* Talanta, 234, 122619. https://doi.org/10.1016/j.talanta.2021.122619

[36] Chakar Khadija, Asdiou Nouhaila, Salhi Anas, Salhi Imane, El Mouden Mahmoud, Hajjaji Abdelowahed, Muthanna H. Al-Dahhan. (2024). *Comprehensive evaluation of TiO_2 nanofluid stability: Insights from pH, EC measurements, and UV-Vis spectroscopy.* Nano-Structures & Nano-Objects, 40, 101387. https://doi.org/10.1016/j.nanoso.2024.101387

[37] María Fernández-Álvarez, Alberto Moure, Luis Angulo Delgado, Julián J. Reinosa, José F. Fernández. (2025).

Raman spectroscopy study of the role of dispersion and interfaces in the improvement of the mechanical properties of epoxy-TiO_2 composites. Journal of Materials Research and Technology, 34, 1744-1758. https://doi.org/10.1016/j.jmrt.2024.12.181

[38] Jiyeon Han, Tiara A M, Seongryeong Kim, Gabriela Morales Florez, Kiran Shrestha, Dang Du Nguyen, Inki Kim, Jinkee Lee & Gyoujin Cho. (2025). *Nanocomposite-based PCR reactors to enhance thermal rate and fluorescence intensity in hand-held qPCR device.* Journal of Nanobiotechnology, 23, 240. https://doi.org/10.1186/s12951-025-03287-0

[39] Yi-Hsing Lin, Hsin-Ta Hsueh, Chia-Wen Chang, Hsin Chu. (2020). *The visible light-driven photodegradation of dimethyl sulfide onS-doped TiO2: Characterization, kinetics, and reaction pathways*. Applied Catalysis B: Environmental, 199, 1-10. https://doi.org/10.1016/j.apcatb.2016.06.024

[40] Pinelopi P. Falara, Nikolaos Chatzikonstantinou, Adamantia Zourou, Polychronis Tsipas, Elias Sakellis, Eleni Alexandratou, Nektarios K. Nasikas, Konstantinos V. Kordatos, Maria Antoniadou. (2025). *Optimizing Carbon Dot—TiO2 Nanohybrids for Enhanced Photocatalytic Hydrogen Evolution*. Materials, 23, 1023. https://doi.org/10.3390/ma18051023

[41] Daniela Herrera Molina, Rubén Antonio Vargas Zapata, Edgar Eduardo Mosquera Vargas. (2020). *Synthesis and characterization of TiO2 nanoparticles and modification of the photodegradation properties by their inclusion in Chitosan (CS).* https://hdl.handle.net/10893/22905

[42] Endang Tri Wahyuni, Titi Rahmaniati, Aulia Rizky Hafidzah, Suherman Suherman,Adhitasari Suratman. (2021). *Photocatalysis over N-Doped TiO2 Driven by Visible Light for Pb(II) Removal from Aqueous Media.* Catalysts, 11, 945. https://doi.org/10.3390/catal11080945

[43] Alamgir, Wasi Khan, Shabbir Ahmad, M. Mehedi Hassan, A.H. Naqvi. (2020). *Structural phase analysis, band gap tuning and fluorescence properties of Co doped TiO2 nanoparticles*. Optical Materials, 38, 278-285. https://doi.org/10.1016/j.optmat.2014.10.054

[44] Gagandeep Kaur, Puneet Negi, Ruhit Jyoti Konwar, Hemaunt Kumar, Nisha Devi, M. Ranjan, K.P. Sooraj, Himitri Trivedi, Bhargav Rajyaguru, N.P. Barde, P.P. Bardapurkar, N.A. Shah, P.S. Solanki. (2025). *Exploring the role of nitrogen doping in tuning the band gap and electrical properties of sol–gel synthesized anatase titanium dioxide nanoparticles*. Optical Materials, 162, 116851. https://doi.org/10.1016/j.optmat.2025.116851

[45] Leonard Moriau, Ivan Marić, Marjan Bele, Anja Logar, Nejc Hodnik, Angelja K. Surca. (2025*). Iridium nanoparticles for oxygen evolution reaction on carbon and TiO_2 supports from a Raman perspective*. International Journal of Hydrogen Energy, 100, 214-221. https://doi.org/10.1016/j.ijhydene.2024.12.337

[46] Katarzyna Kołodziejak, Adrian Niewiadomski, Hańcza B. Surma, Jarosław Sar, Piotr Piotrowski, E. Talik, Dorota A. Pawlak. (2024). *3D network of MnTiO3–TiO2 eutectic composite studied by Raman spectroscopy.* Journal of Solid State Chemistry, 338, 124839. https://doi.org/10.1016/j.jssc.2024.124839

[47] Maryam Ahmadi, Seyed Mehdi Alavi, Afsanehsadat Larimi. (2023). *UV–vis light responsive Bi_2WO_6 nanosheet/TiO_2 nanobelt heterojunction photo-catalyst for CO_2 reduction*. Catalysis Communications, 179, 106681. https://doi.org/10.1016/j.catcom.2023.106681

[48] Vassilios Binas, Danae Venieri, Dimitrios Kotzias, George Kiriakidis. (2020). Modified TiO2 based photocatalysts for improved air and health quality. Journal of Materiomics, 3, 3-16. https://doi.org/10.1016/j.jmat.2016.11.002

[49] Huan Wang, Bokai Liao, Yuebin Xi, Yunhui Feng, Huixiang Wu. (2022). Excellent fluorescence and photoelectricity of TiO2/Au/PS enabled by a synergistic carrier transfer effect. Materials Letters, 320, 132344. https://doi.org/10.1016/j.matlet.2022.132344

[50] Dorah Kawira Muthee, Francis Birhanu Dejene, Lawrence Kioko Munguti. (2025). Modification of TiO2 anatase-rutile mixed-phase properties using Sn4+ doping for photocatalytic brilliant green degradation. Applied Catalysis A: General, 695, 120166. https://doi.org/10.1016/j.apcata.2025.120166

[51] Qiangang Li, Guo-hua Liu, Lu Qi, Hongchen Wang, Guang Xian. (2023). Chlorine-mediated electrochemical advanced oxidation process for ammonia removal: Mechanisms, characteristics and expectation. Science of The Total Environment, 896, 165169. https://doi.org/10.1016/j.scitotenv.2023.165169